ADVANCED MATERIALS
www.advmat.de

Stretchable Thin Film Mechanical-Strain-Gated Switches and Logic Gate Functions Based on a Soft Tunneling Barrier

Soosang Chae, Won Jin Choi, Ivan Fotev, Eva Bittrich, Petra Uhlmann, Mathias Schubert, Denys Makarov, Jens Wagner, Alexej Pashkin, and Andreas Fery**

Mechanical-strain-gated switches are cornerstone components of material-embedded circuits that perform logic operations without using conventional electronics. This technology requires a single material system to exhibit three distinct functionalities: strain-invariant conductivity and an increase or decrease of conductivity upon mechanical deformation. Herein, mechanical-strain-gated electric switches based on a thin-film architecture that features an insulator-to-conductor transition when mechanically stretched are demonstrated. The conductivity changes by nine orders of magnitude over a wide range of tunable working strains (as high as 130%). The approach relies on a nanometer-scale sandwiched bilayer Au thin film with an ultrathin poly(dimethylsiloxane) elastomeric barrier layer; applied strain alters the electron tunneling currents through the barrier. Mechanical-force-controlled electric logic circuits are achieved by realizing strain-controlled basic (AND and OR) and universal (NAND and NOR) logic gates in a single system. The proposed material system can be used to fabricate material-embedded logics of arbitrary complexity for a wide range of applications including soft robotics, wearable/implantable electronics, human–machine interfaces, and Internet of Things.

1. Introduction

Starting with the invention of the transistor in 1947, integrated circuits have unleashed changes comparable to the Industrial Revolution by making the computer revolution and the Information Age possible.[1] Similarly, mechanical-strain-gated electronic components and their implementation in integrated logic circuits enable a new materials science concept, where decisions are carried out on the material level without the use of conventional electronic components. This concept has appealing application scenarios in mechanosensitive electronics, including flexible and highly deformable electronics and devices,[2,3] electronic skin,[4–6] implantable sensors for health monitoring,[7,8] and soft actuators/robotics,[9–11] among others. A full-fledged mechanical logic gate requires the same material system to demonstrate three distinct operation modes

S. Chae, E. Bittrich, P. Uhlmann, M. Schubert, A. Fery
Leibniz-Institut für Polymerforschung Dresden e.V
Hohe Straße 6, 01069 Dresden, Germany
E-mail: chae@ipfdd.de; fery@ipfdd.de

W. J. Choi
Department of Materials Science and Engineering
University of Michigan
Ann Arbor, MI 48109, USA

I. Fotev, D. Makarov, A. Pashkin
Helmholtz-Zentrum Dresden-Rossendorf e.V.
Institute of Ion Beam Physics and Materials Research
01328 Dresden, Germany

I. Fotev, A. Fery
Technische Universität Dresden
01062 Dresden, Germany

The ORCID identification number(s) for the author(s) of this article can be found under https://doi.org/10.1002/adma.202104769.

DOI: 10.1002/adma.202104769

P. Uhlmann
Department of Chemistry
University of Nebraska-Lincoln
Lincoln, Nebraska 68588, USA

M. Schubert
Deprtment of Electrical and Computer Engineering
University of Nebraska-Lincoln
Lincoln, NE 68588, USA

M. Schubert
Department of Physics
Chemistry and Biology
(IFM)
Linkoping University
Linkoping 58183, Sweden

J. Wagner
Chair for Circuit Design and Network Theory
Technische Universität Dresden
01062 Dresden, Germany

J. Wagner
Centre for Tactile Internet with Human-in-the-Loop (CeTI)
Technische Universität Dresden
01062 Dresden, Germany

upon mechanical deformation, which can identically respond against any external mechanical constraints. Specifically, in addition to enabling a strain-invariant conductor, which will not exhibit a change in electrical conductivity when stretched, the material system should enable two switch elements; upon application of strain, these switches should turn the circuit on (transition from an insulating to a conducting state, functioning as an "on-switch") or off (transition from a conducting to an insulating state, functioning as an "off-switch"). Although the literature contains numerous reports of both stretchable strain-sensing elements[12–20] and stretchable conductors,[21–27] the bottleneck in this field is still the lack of a facile approach for integrating strain-gated logic functionality within the same material system. Most importantly, the key to a strain-gated logic circuit is a strain-gated electronic on-switch. This unique functional element undergoes a transition from insulating to conductive behavior when subjected to tensile strain. In this respect, it functions like a transistor in a conventional electronic circuit.

Stretchable strain-gated electronic switches might be realized through the development of stretchable piezoresistive composites containing a percolated network of a conductive filler in an elastomeric matrix. However, the percolated network in composites under applied strain tends to break, resulting in an increase in the composites' electrical resistance.[28] This behavior is typical of systems with a positive piezoresistive effect (i.e., only an off-switch feature). Stretchable composites featuring negative piezoresistivity, which are needed for the realization of strain-gated electronic on-switches, have rarely been reported and require a negative piezoresistive filler embedded in an elastomeric matrix.[29–31] Entangled conducting polymer composites and carbon-fiber-reinforced polymers (CFRPs) have shown negative piezoresistivity because of an increase in the degree of alignment under applied strain.[32] However, the state-of-the-art negative piezoresistive composites exhibit a poor on-to-off ratio (less than 10^3 to 10^4) and a narrow operating strain range (less than 3–4%), which limits their applicability in highly deformable electronics intended for use in on-skin devices and soft robotics.

A mechanical-force-gated electric switch fabricated by prepatterning a metal microstructure on an elastomeric substrate and operated by compressive deformation has recently been proposed.[33–35] The requirement that the microstructure should be formed in advance as well as the less favorable compressive instead of tensile operation introduce additional challenges when considering high-density integration of a circuit for skin-compliant electronics.

Here, we report a stretchable strain-gated electric switch based on a bilayer metal thin film sandwiching an ultrathin 12 nm-thick elastomeric insulator barrier layer. The use of an ultrathin elastomer as a tunneling barrier material between two electric conductors enables the quantum mechanical transparency of the barrier to be tuned via quantum-scale thinning by application of mechanical tensile strain in a range as large as 130%. We demonstrate that, upon application of strain, the conductivity between the electrically contacted bilayer undergoes a transition from $\sigma_{\varepsilon=0} \approx 10^{-5}$ S cm^{-1} at zero strain to $\sigma_{\varepsilon=1.0} \approx 10^{4}$ S cm^{-1} at unity strain. Because the thickness of the bimetal layer and soft barrier layer can be controlled, the material system enables the fabrication of all three functional elements of mechanical-strain-gated logic circuits: the on- and off-type switches and the strain-invariant interconnects (see schemes in **Figure 1**). By combining these elements, we demonstrate four stretchable strain-gated logic gates including basic (AND and OR) as well as universal (NAND and NOR) gates in a single thin film material system (see schemes and digital photograph in Figure 1a). This work provides a viable materials science platform that can perform logic operations of arbitrary complexity without using conventional electronic components. This technology has strong potential for use in the emerging applications of soft electronics and soft robotics, including skin-compliant electronics for interactive human–machine interfaces, as well as in medical applications such as wearable and implantable health monitors.

2. Design of the Sandwiched Bilayer Metal Thin Film with a Soft Thin Barrier Layer

To achieve stretchable mechanical-strain-gated electric switches, we developed a strategy to prepare an ultrathin poly(dimethylsiloxane) (PDMS) spacer sandwiched between two Au thin-film electrodes (Figure 1 and **Figure 2**a). The PDMS layer acts as an insulating soft tunnel barrier (scheme Figure 2b). The layers are sequentially stacked on the substrate (see details in the Experimental Section, and Section S1 and Figure S1, Supporting Information). The thin-film fabrication technology enabled precise control of the metal layer thickness and enabled us to exploit the percolation threshold at which the thin metal film transitions from conductive to insulating behavior. Hence, by optimizing the deposition thickness and controlling the fabrication conditions of the elastomeric tunneling barrier layer, we obtained a stretchable composite possessing all three essential functionalities needed for strain-gated logic devices: on-switch, off-switch, and stretchable interconnect (see schemes in Figure 1b–d). In particular, such an optimized combination of the three functionalities enables the fabrication of basic and universal logic gates, all in 50 nm stretchable metal thin form, in a single material system.

3. Mechanism of Strain-Gated Electric Switches

Under an applied strain, the PDMS soft barrier layer becomes thinner, whereas it increases in length along the strain direction. Although the gaps between the intrametal domains in both layers may also increase (scheme in Figure 1b), the thinning leads to a tunneling current across them (right scheme in Figure 2b). We conducted terahertz time-domain spectroscopy (THz-TDS) measurements on a stretched PDMS sample to evaluate the thinning of the PDMS layer as a function of strain (Figure 2c, red line, details in the Experimental Section, and Section S2 and Figure S2, Supporting Information). Knowing the thickness variation of the PDMS layer under strain, we modeled the conductance (j) of the structure using the tunneling model proposed by Simmons[36] (see Section S2, Supporting Information, for calculation details)

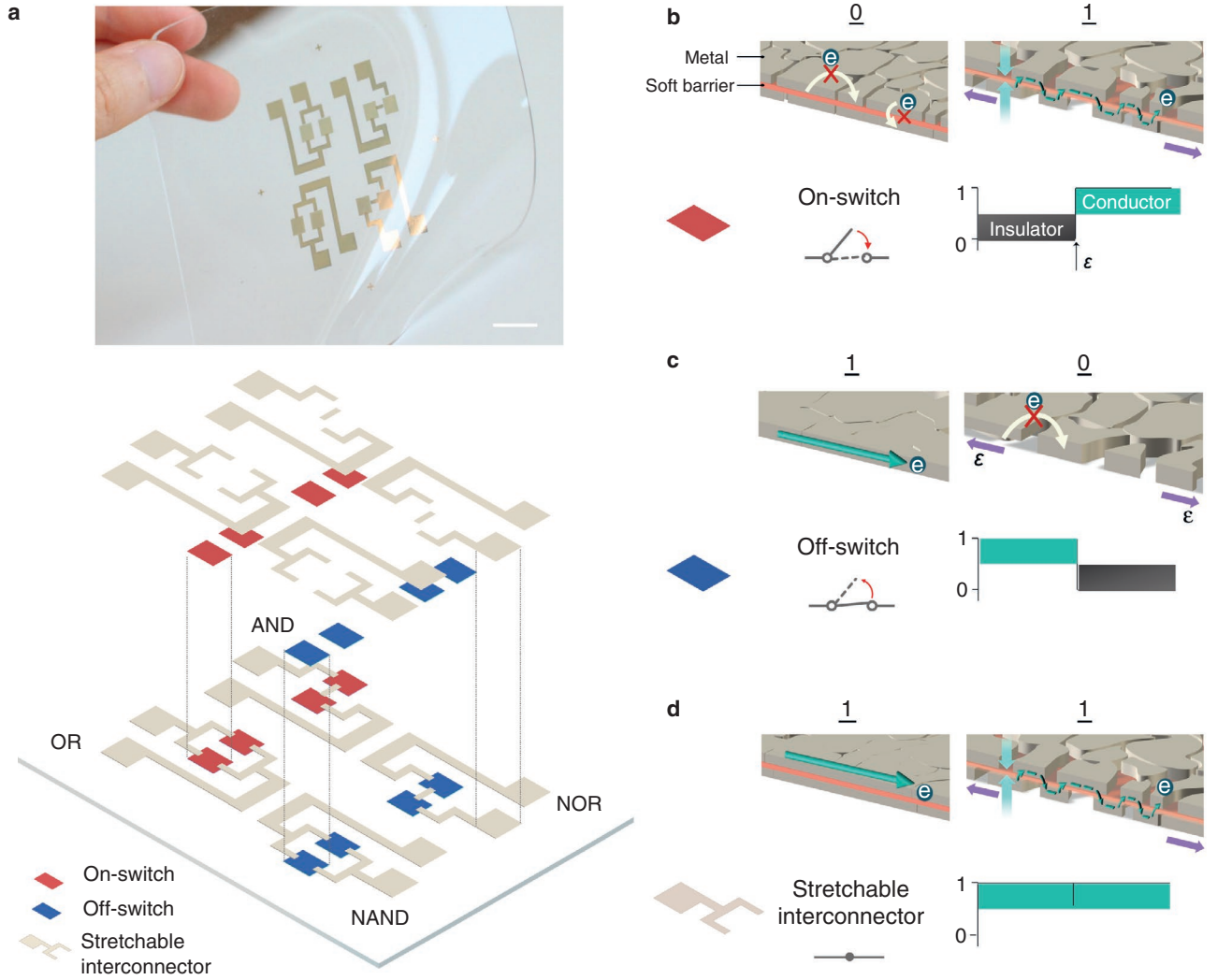

Figure 1. Sandwiched bilayer metal thin film with a soft barrier layer for all types of stretchable mechanosensitive electric components and for fabricating thin-film mechanical-strain-gated logic circuits. a) With precise control of the deposition thickness of the bimetal thin film (e.g., percolation conditioning) and quantum-scale thinning of the soft barrier layer upon stretching (details in Figure 3), the designed structure demonstrates all three modes of stretchable strain-gated electric components: from top to bottom of scheme. b) "On-switch" (insulator-to-conductor transition upon stretching, marked as 0 and 1, respecitvely), c) "off-switch" (conductor-to-insulator transition upon stretching), and d) stretchable interconnector (constant conductor upon stretching). In particular, for the on-switch function, an extremely high on/off electrical conductivity ratio was obtained over a wide range of working strains. All three configurations can be used to realize a fully stretchable mechanical-strain-gated logic gate in a single thin-film system ((a) and digital image; scale bar: 1 cm).

$$j = \frac{\sqrt{2m\varphi}}{s(\varepsilon)}\left(\frac{e}{h}\right)^2 V \exp\left[-\frac{4\pi s(\varepsilon)}{h}\sqrt{2m\varphi}\right] \quad (1)$$

where $s(\varepsilon)$, e, m, φ, V, and h are the barrier thickness dependent on strain (ε), the charge of an electron, the mass of an electron, the barrier height, the voltage across the two terminals, and Planck's constant, respectively. The calculated conductance of the switch device is shown in Figure 2c, together with the measured values. The barrier height of the PDMS layer was set to $\varphi = 2.3$ eV to achieve the best agreement with the experimental data. Obviously, for $\varepsilon > 0.5$, the conductance saturates and does not demonstrate the model's prediction of exponential growth with increasing strain. We speculate that, at such large strain, the thin PDMS barrier layer begins to slip and loses its bonding with the substrate. As a result, the barrier thickness does not vary as the applied strain is increased further, leading to the observed current saturation.

Presumably, the lateral conductivity (via intraconduction) also must change at such large strain regions, thus could be decreased again due to the reduction of the number of metal islands per unit area upon further stretching. This issue could be more pronounced in the microminiaturized device. As will be described in detail in Section 5, further studies using thicker metal and intermediate layer to increase the specific number of metal island per unit area can be performed to increase the overstretching limitation (Figure S19, Supporting Information). For other future material configurations, as evident from

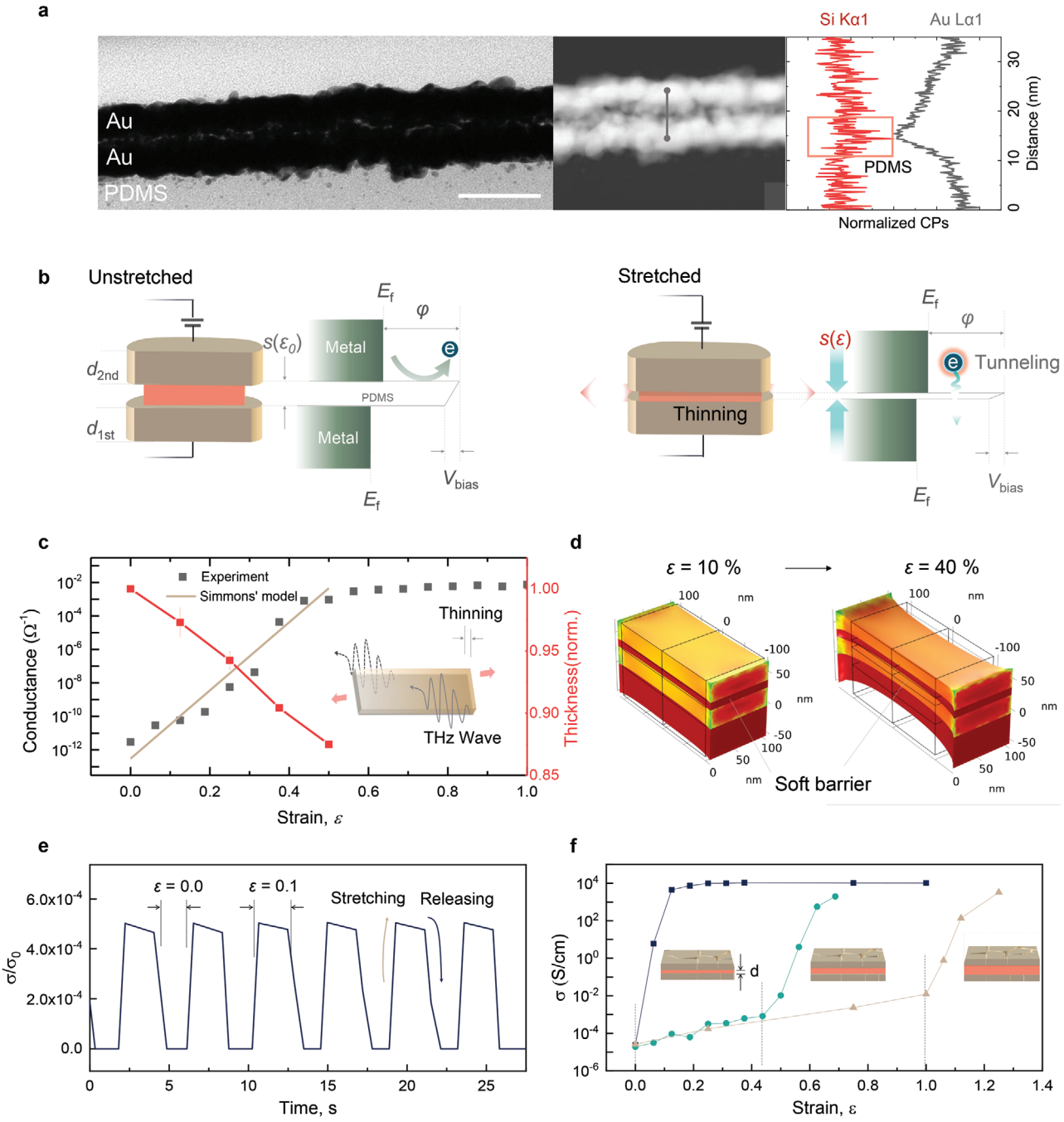

Figure 2. Working principle of the strain-gated electric switch: tunneling current caused by thinning of the soft barrier layer. a) A bimetal layer (each 20–30 nm thick) and thin soft insulator barrier layer (≈12 nm thick); scale bar, 100 nm. (Right) Scanning TEM image of the device and line profile of the energy-dispersive X-ray spectra of Si and Au atoms for identifying the soft barrier layer (e.g., PDMS) sandwiched in the metal thin-film bilayer (e.g., Au). b) Expected energy-level diagrams of a stretchable electric switch in the unstretched (left) and stretched (right) states, where electrons transport through the thinned barrier layer caused by stretching (s_ε), whereas no electron transport occurs because of the sufficient thickness ($s\varepsilon_0$) with a high barrier height (φ) in the absence of stretching. c) Strain-dependent conductance with experimentally measured thinning of the soft barrier layer, as measured by THz-TDS (red line). Measured conductance of a stretchable switch sample (black dots) and the calculation according to the low-voltage-limited Simmons' tunneling equation, Equation (1) (brown line). d) Theoretical thinning of the soft barrier layer simulated by the finite element method (Figure S3, Supporting Information). e) Reversible strain-dependent conductivity in the $\varepsilon = 0.1$ strain regime. f) Modulation of threshold strain of the off-to-on transition by controlling the initial thickness of the tunneling barrier (details in Section S5, Supporting Information).

Figure S6 (Supporting Information), both the initial thickness of the barrier layer (s_0) and the barrier height (φ) between the metal–barrier interfaces jointly determine the on-to-off ratio: larger on-to-off ratios are expected for thicker and higher barriers. The on-to-off ratio remains constant from the first to the final cycle (Figure 2e and Figure S7, Supporting

Information), and this behavior was found to be completely reversible, which is direct experimental evidence of the tunneling mechanism. In addition, by varying the initial thickness of the PDMS barrier layer, we modulated the turn-on strain of the switch (Figure 2f and Section S5, Supporting Information). This feature is advantageous for extending the range of applications, especially in scenarios that require different threshold strains. Notably, the experimental data are comparable to the results obtained via a finite element simulation (Figure 2d; Section S3 and Figure S3, Supporting Information).

By adjusting the thickness of both metal layers, we tailored not only the on-switch performance but also fabricated the other complementary circuit components; off-switches and strain-invariant interconnects. The Au thin films are brittle and readily form cracks and lose their electrical conductivity when the underlying elastomer substrate is stretched. Thus, the same bilayer metal thin film without a soft tunneling layer demonstrated off-switch behavior (see scheme in Figure 1c and Figures S8 and S9, Supporting Information). Governed by the deposition thickness (i.e., the percolation mechanism shown in the scheme in Figures S10 and S11, Supporting Information), the bilayer structure for the mechanical-strain-gated electric on-switch was electrically isolated at the beginning because the intra-conduction path was disallowed as a consequence of insufficient deposition thickness; at the same time, the soft barrier layer with a potential barrier of appropriate height was sufficient to prevent a tunneling current between the metal layers (scheme in Figures 1b and 2b). Meanwhile, the sufficient deposition thickness of the second layer for the stretchable conducting interconnector enabled electrical conduction even at the beginning when it was used as a stretchable interconnector (scheme in Figure 1d).

Upon the application of strain in both configurations, the thickness of the thin soft barrier decreased because of the strain, governed by the Poisson effect. This decrease in thickness was followed by electron tunneling currents through the barrier, forming an interconnected bilayer metal electrode, as described in the discussion of the tunneling mechanism. Experimentally, to elucidate such an effect of the metal layer thickness with respect to the percolation mechanism on the strain-dependent electrical properties, the change in conductivity of the bilayer structure at applied strains ($0 \le \varepsilon \le 0.31$) was plotted for various deposition thicknesses of both layers (the first metal layer, d_{1st}, and the second metal layer, d_{2nd}) as a contour plot in **Figure 3**a. The corresponding changes in conductivity for the full range of strain ($0 < \varepsilon < 1.0$) and the change rate, $\frac{d(\log \sigma^{-1})}{d\varepsilon}$, are shown in Figure 3b–d. Note that only thickness region *C* shows the feature of the on-switch, $\sigma_{\varepsilon=0} > 10^{-5}$, $\sigma_{\varepsilon=0.06} \approx 10^{-3}$, $\sigma_{\varepsilon=0.12} \approx 10^{-1}$, $\sigma_{\varepsilon=0.18} \approx 10^{2}$, and $\sigma_{\varepsilon=0.31} < 10^{4}$ S cm^{-1}; the other thickness regions maintain a constant conductivity of either greater than 10^{4} S cm^{-1} (region B) or less than 10^{-5} S cm^{-1} (region A) irrespective of applied strain. As previously been explained in the discussion of the percolation mechanism, region *C* well matches the percolation threshold thickness for each metal layer (Figure S12, Supporting Information). Likewise, the devices within region B exhibit strain-invariant conductivity (>10^{4} S cm^{-1}) to ε = 100%, which implies that the material system can also be used as an interconnect for on- and off-switches in stretchable strain-gated logic circuits. These systems exhibit excellent stretchability as well as a great cyclic stability. On-switching performance as a function of repeated stretching and releasing cycles up to 5000 at a given applied strain ($\varepsilon = 10\%$) was shown in Figure S18 (Supporting Information). The operation of on-switching upon stretching remains unchanged after the initial training phase of about 1500 stretching cycles. For the stretchable interconnector, its initial electrical conductivity fully maintained for 1000 cycles of 100% strain as shown in Figure S13 (Supporting Information).

4. Demonstration of Thin-Film Stretchable Integrated Mechanical-Strain-Gated Logic Circuit

We compared the strain-dependent absolute DC conductivity of our sandwiched bilayer metal thin film with a soft barrier layer (Figure S14, Supporting Information) across the stretchable conductors in the literature;[21–27] this characteristic can be the most important characteristic for realizing strain-gated functional elements. When the electrode is in the "off" state (i.e., in the absence of strain), the initial conductivity of our device is almost outside the measurable range ($\sigma_{\varepsilon=0} = 10^{-5}$ S cm^{-1}). When the electrode is in the "on" state (i.e., when a strain of $\varepsilon > 50\%$ is applied), the conductivity exceeds that of other stretchable electrodes reported elsewhere.[21–27] Electrical conduction in our structure in the stretched state can occur between the two metal thin films without any interruption from the insulating matrix, resulting in a superior on-state conductivity ($\sigma_{\varepsilon=1.0} = 10^{5}$ S cm^{-1}) comparable to that of pristine bulk metals (e.g., Ag and Au, > 10^{6} S cm^{-1}).

Given these characteristics, our stretchable electrodes outperform the state-of-the-art solutions with respect to electrical conductivity and stretchability. As a demonstration, we visualized the mechanosensitive electrical performance of three of our selected devices (**Figure 4**). Their high-conductivity switching dynamic (with corresponding *I*–*V* curves) was demonstrated by the devices either fully conducting the current necessary to operate a light-emitting diode (LED) irrespective of strain (stretchable strain-invariant interconnect, Figure 4c), operating at zero strain while blocking the LED current at nonzero strain (off-switch, Figure 4b), or operating at nonzero strain while blocking the LED current at zero strain (on-switch, Figure 4a and Movie S1, Supporting Information).

To demonstrate the potential of our material system for strain-gated logics, we fabricated four logic gates activated by strain, including basic AND and OR gates as well as universal NAND and NOR gates. To assemble the logic gates, we combined on- and off-switches and connected them using strain-invariant interconnects into a single device (the actual operating logic circuit in **Figure 5**a and the microscale miniaturized model circuit in Figure 5b). Notably, all four of the logic gates were less than 50 nm thick (thickness data in Figure S15, Supporting Information); they can thus be used to realize more sophisticated logics in material-embedded circuits. When two on-switches and two off-switches were connected in series and parallel, the logic output operated AND/OR and NAND/NOR, respectively (Figure 5c). For the inputs, strained ($\varepsilon > 20\%$) and

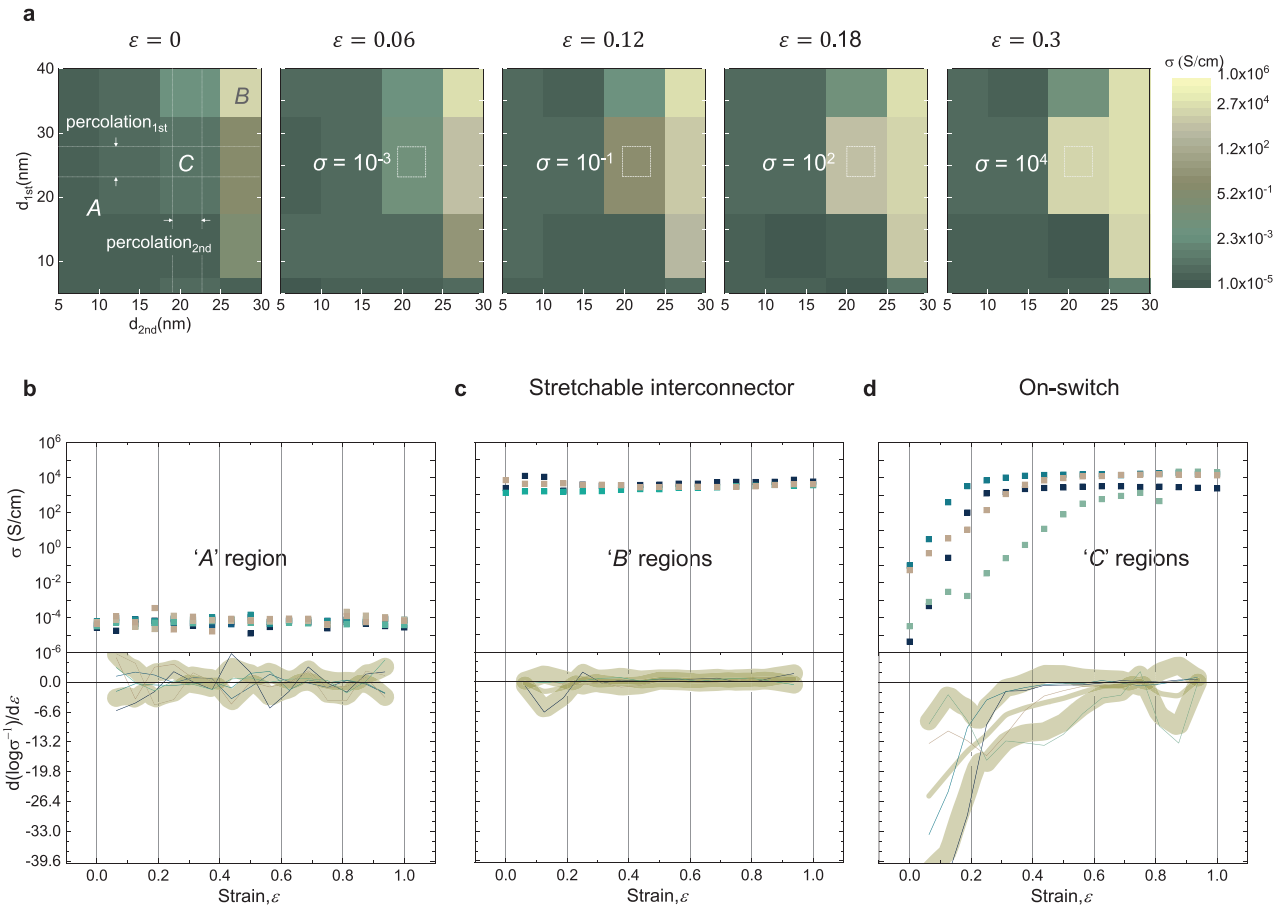

Figure 3. Thickness effect of the metal layer on switching behavior. a) The switch behavior is dependent on the thickness of the bimetal layer. For different combinations of the two-layer thicknesses (vertical axis: first layer; horizontal axis: second layer), the change tendency of conductivity in the bilayer electrode with various strains (ε = 0, 0.06, 0.12, 0.18, 0.3) was classified as constant insulator-like (*A* combination); constant metal-like conduction, stretchable interconnector (*B* combination); and transition from insulator-like to a metal-like conduction, strain-gated electric switch (*C* combination), where the percolation thickness of each metal layer was the criterion for determining the classification (Figures S10–S12, Supporting Information). b–d) The conductivity change of respective regions in the full range of applied strain ($\varepsilon = 0 \rightarrow 1$) and the corresponding rate of change for the *A* combination (b), the *B* combination (c), and the *C* combination (d). A stretchable device satisfying combination *C* shows the dramatic transition in conductivity only under applied strain, i.e., strain-gated electric on-switching behavior.

unstrained ($\varepsilon = 0\%$) states were defined as 1 and 0, respectively (Figure 5d), whereas the output was assigned in terms of the overall current density across the GND and OUT pads, with conductive and nonconductive states corresponding to 1 and 0, respectively (Figure 5c,d). The AND logic device showed a nonconductive 0 state as the output in all cases except when both inputs were loaded (1,1), which led to the connection of only mechanical-strain-gated on-switches at both inputs and therefore to a connection in the overall conductive pathway across the logic device (Figure 5a). By contrast, a parallel connection between the on-switches acted as an OR gate. The device demonstrated a conductive "1" output for all of the inputs except when both inputs were loaded (0,0), which led to disconnection in the overall conductive pathway across the device. Although it is sufficient to use only on-switches to realize AND and OR logic gates, more advanced NAND and NOR gates are based on off-switches: the operations are performed vice versa to AND/OR gates (Figure 5c). As a result, depending on the combination of the input strain, the output current of each logic gate showed distinct signal levels (Figure 5d).

5. Perspective and Outlook

We demonstrated that the nanometer-scale sandwiched bilayer Au thin film with an ultrathin polydimethylsiloxane elastomeric barrier layer is a promising platform to bring the high potential of mechanical-strain-gated stretchable electric switches. Thanks to their outstanding performance of off-to-on ratio of on-switch, and universality for fabrication of off-switch and stretchable interconnector, these new materials design appears to be especially suitable for prospective development of stretchable mechanical-strain-gated logic circuit. One of the challenges, which are still to be addressed is the performance of the on-switch at strains of larger than 50% and further improvement of the long-term cyclic stability. Several routes can be proposed to overcome these issues. In the present work, spontaneous diffusion behavior of low-molecular weight PDMS species is used to form an ultrathin soft elastic barrier layer (see details in the Experimental Section), by which enabled highly reliable and uniform thin layer even without additional coating process. The impact of an additional adhesive layer between the PDMS

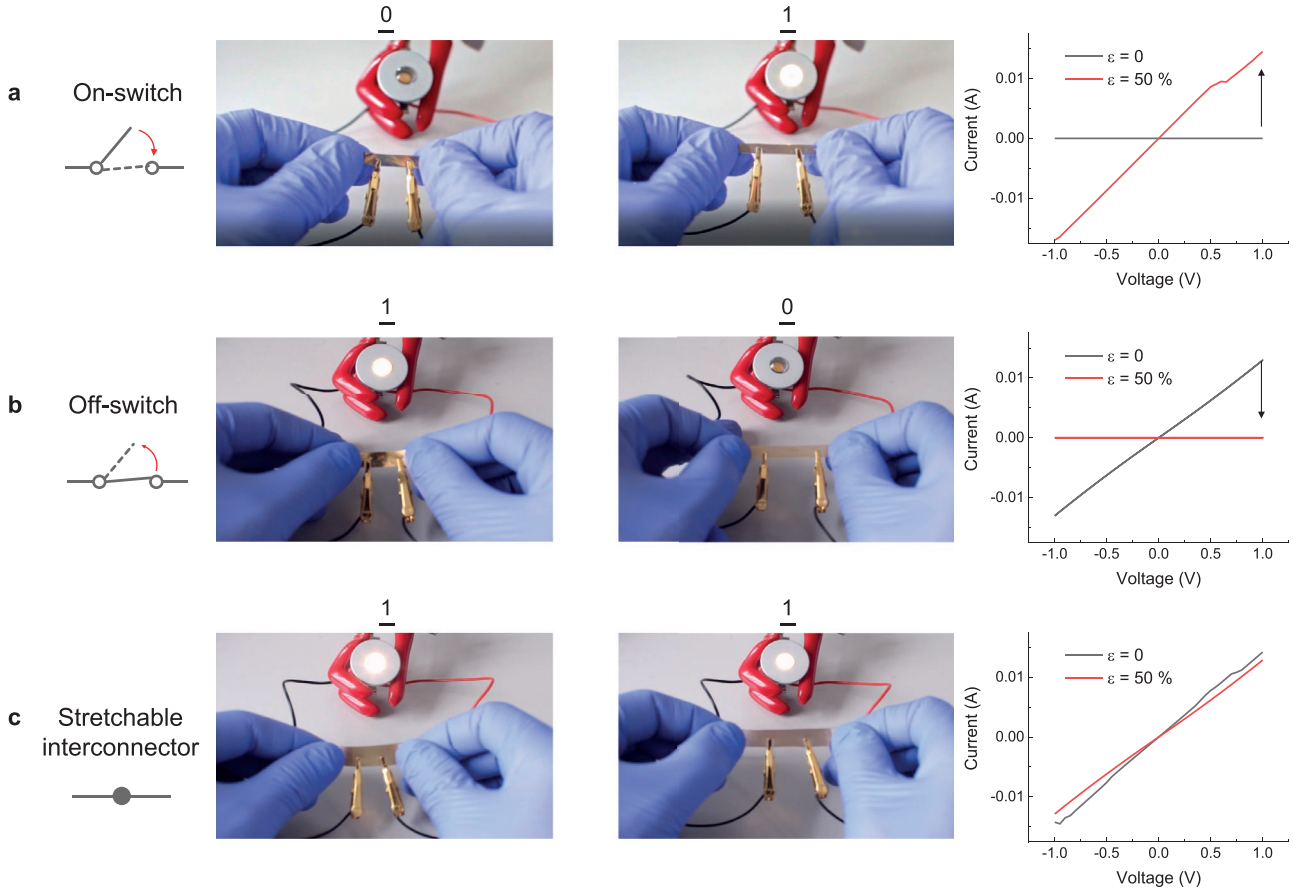

Figure 4. Mechanical-strain-gated stretchable electric device. Switching-on and switching-off test of a light-emitting diode (LED) bulb and the corresponding *I–V* curves for various stretched mechanical-strain-gated electric devices, which can potentially be used as the three basic components of a mechanical-strain-gated logic circuit (left: without stretching; right: with stretching to 50%). a,b) The results show a dramatic transition from insulator-like to metal-like conduction (on-switch) and from metal-like to insulator-like conduction (off-switch), respectively, and c) superior constant electrical stretchability under stretching (stretchable interconnector). The design achieves versatility through precise control of the experimental parameters in a single system of thin films.

and the first metal layer on the mechanical performance of the on-switch is still to be explored. Furthermore, the long-term cyclic stability could be improved by introducing of an adhesion layer (thin Ti or Cr) between the interfaces.[37] The crack formation in the metal layers could be minimized by decreasing the lateral size of metal clusters, instead of a more flake-like ones used in this work. Controlling the surface crosslinking density of the PDMS substrate is crucial for determining the feature of the deposited metal continent,[38] which could be conditioned to obtain the metal flake with a smaller size. Another important aspect is the prevention of the conductivity decrease when the on-switches are stretched beyond 50% applied strain. We attribute this effect to the reduction of metal cluster density upon overstretching. This issue can be overcome by the use of a thicker metal layer than current bi-layer design, thus giving higher metal cluster per unit area.

Soft electric devices enable strain/motion sensing on human skin and are among the most promising alternatives to the established optical-based motion tracking technology. Despite the obvious application potential of such a device as on-skin strain sensors based on various stretchable conductor/sensing materials, the sensor configuration for converting a mechanical input into an electrical output signal is still based on conventional Wheatstone bridges, which are typically used in strain-gauge measurements on stiff materials. Although the Wheatstone bridge method is straightforward for measuring the strain value on a rigid and stiff body, it is not appropriate for tracking a continuous and complex motion of soft matter. For instance, the method is limited to tracking simple on-off motions such as the spreading and folding of fingers/arms.[39] Hence, the sensing resolution is relatively poor—at the level of a few centimeters.[40] To overcome the limited resolution of the Wheatstone bridge method, our work paves the way towards the advanced mode of a stretchable mechanical gated logic circuit that can be integrated into a micromodule and that can be seamlessly integrated with human tissues to sense complex deformation with high intimate interaction between the device and the tissues.

6. Conclusion

The proposed bilayer metal thin film with an intermediate thin soft insulator layer on a stretchable substrate exhibits

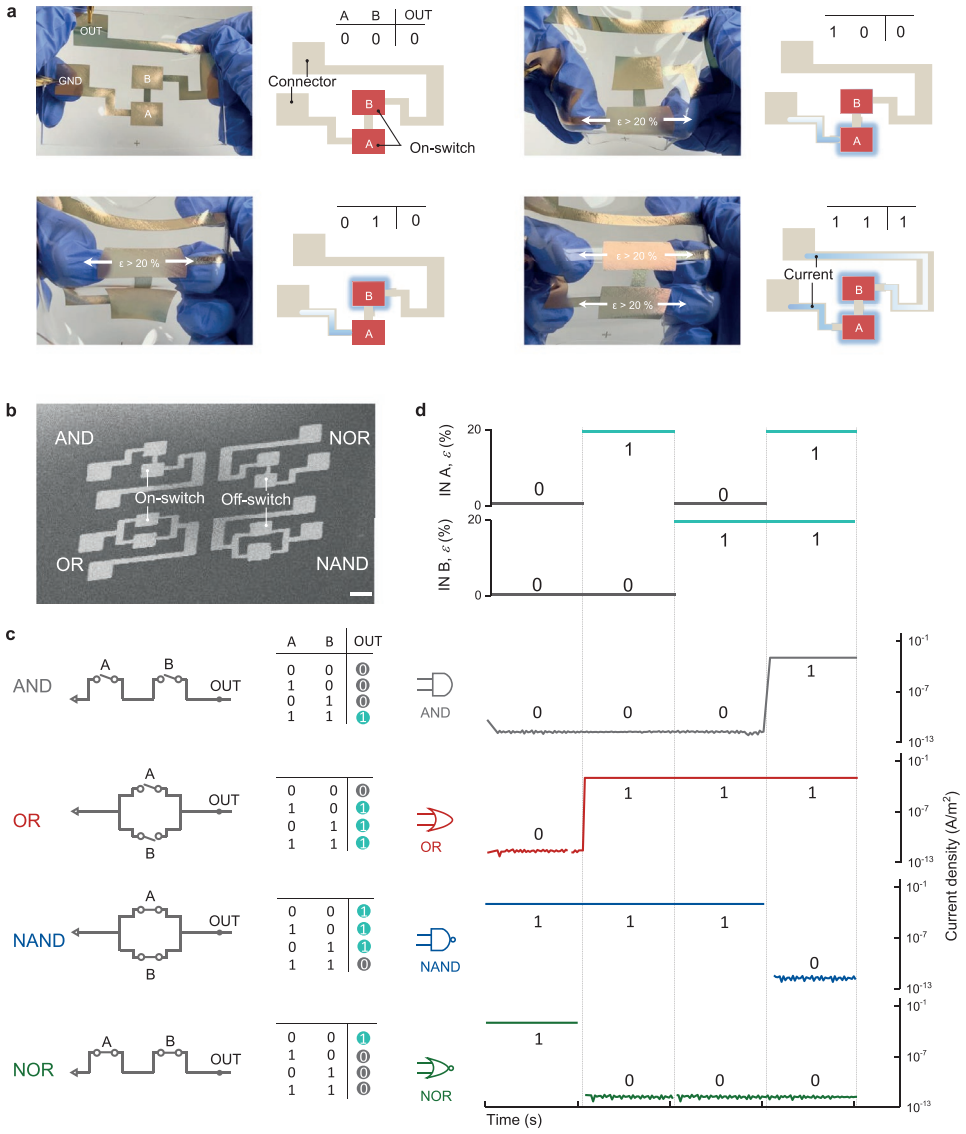

Figure 5. Demonstration of mechanical-strain-gated stretchable thin-film logic gate. a) Fully stretchable AND mechanical-gated logic by incorporating both the on-switch (for the area of the mechanical gating) and stretchable interconnector (for the area of strain-invariant connector and wiring pad). Upon the application of strain ($\varepsilon > 20\%$), logic levels of "0" and "1" correspond to nonconductive and conductive of the on-switch, respectively. b) As-fabricated microscale model logic gates, including AND, OR, NAND, and NOR (scale bar: 100 µm) in a single thin-film material system (<50 nm, Figure S16, Supporting Information) capable of the sophisticated micromodule integration. c) Schematic of fabricated complementary four-logic gates formed by connecting two on- and off-switches in series and parallel configuration together on a PDMS substrate, with a stretchable interconnector (see scheme in Figure 1a and Figure S15, Supporting Information). d) The application and release of strain ($\varepsilon > 20\%$) on each switch (*A* and *B*) are set to input 0 and 1, respectively. Four logic gates (from top to bottom) can produce different outputs (different current densities) that are distinguishable between the conductive ("1" output) and insulating ("0" output) state depending on the different combinations of the input strain of *A* and *B* on the on- and off-switches.

a drastic change in conductivity under applied mechanical strain. Starting from insulator-like conductivity (10^{-5} S cm^{-1}), it exhibits an extremely high on/off ratio (≈10^9); metal-like conductivity (10^4 S cm^{-1}) is achieved under an applied strain as high as 130% in the on-switch device. Tuning the thickness of the metal layer or omitting the soft intermediate layer enables the design to be readily converted to stretchable strain-invariant interconnects and the opposite type of switch (off-switch). By combining these functional elements, we fabricated four strain-gated logic elements that rely on the same mechanically stretchable material system. This work introduces the possibility of integrated strain-gated logic circuits that precisely capture mechanical deformation even on arbitrary soft matter and that are particularly suitable for human–machine interfaces for interactivity with surroundings, smart implants, and wearable health monitors.

7. Experimental Section

PDMS Preparation: The PDMS substrate was prepared by mixing PDMS prepolymer (Sylgard 184, Dow Corning) with a curing agent (Sylgard 184, Dow Corning) at a 10:1 weight ratio. The resultant mixture was poured into a flat Petri dish, maintained at room temperature for 8 h, and then thermally cured at 35 °C for 12 h. The cured PDMS slab

with 1.0 mm thickness was used as a substrate and as a reservoir for the diffusion of PDMS to form an intermediate PDMS layer, with no further treatment. The diffusion of low-molecular-weight PDMS from the PDMS substrate through the first deposited metal layer led to the spontaneous formation of a thin PDMS layer on the surface of the first metal layer. The diffusion process generally takes a few weeks when the sample is kept at atmospheric pressure. To accelerate this process, cracking of the first metal thin film was induced, and the sample was incubated under high vacuum, which dramatically decreased the diffusion time of the PDMS. For practical approach, after an Au thin film was deposited onto the PDMS substrate, the sample was stretched to 80% strain to induce cracks in the Au thin film. The sample was kept under a reduced pressure of 6.0×10^{-6} mbar for 8 h, which is optimized for the high performance of switching devices (more details in Section S1, Supporting Information). The initial thickness of the intermediate PDMS tunneling barrier was determined by spectroscopic ellipsometry (more details in Section S4, Supporting Information).

Au Thin-Film Deposition: The PDMS substrate was mounted onto a sample holder for PVD (chamber: Hex, Korvus Technology), and an Au thin film was deposited by thermal evaporation. The deposition rate was 0.3 Å s^{-1} with the deposition chamber evacuated to a pressure less than 6.2×10^{-6} mbar. The thickness was monitored in situ by quartz crystal microbalance.

Electrical Characterization Measurement: A Keithley 2612B sourcemeter was used for the DC electrical conductivity and resistivity measurements of all samples. The probe station (TS50, MPI AST) was equipped with a four-point probe tip of tungsten. The specimens for the resistivity and conductivity calculations were defined within an area of 1 cm × 1 mm, and the leads of the probe tip were directly connected to the pristine surface of samples. The tips were attached and detached onto stretched sample surfaces to maintain the distance between each tip. For the real-time strain sensor, measurement of a silicone conductor (RTV-SNC-015, Euro Technology) was used to sustain the electrical contact during the strain-release cycle.

Characterizations: All of the atomic force microscopy images were obtained with an MFP-3D atomic force microscope (Asylum Research, USA). For the cross-sectional transmission electron microscopy (TEM) images, the strain-gated electric component sample was prepared as lamellar thin slices by focused ion beam (FIB) (JIB-4601F, JEOL); TEM analysis was then conducted (JEM-ARM 200F, JEOL). For the cross-sectional scanning electron microscopy (SEM) analysis (NEON40, ZEISS), various thicknesses of the samples were cross-sectioned by FIB. THz-TDS measurements were performed using a homemade setup based on a Ti:sapphire femtosecond laser amplifier (Coherent RegA 9000), a photoconductive GaAs THz emitter, and a ZnTe electro-optic detector. The covered spectral range was 0.3–2.7 THz. For a series of confocal microscopic images under applied strain in situ, the strain-gated electric component samples were mounted onto a homemade motorized linear stage (L505, PI) and the stage was placed under a Nanofocus confocal microscope. Water contact angles on the sample surfaces were measured using DataPhysics OCA35L. Thin PDMS layer thicknesses were obtained by modeling ellipsometric data (M2000-UI, J.A. Woollam Co. Inc., USA) using a fixed-refractive-index dispersion of $n(\lambda) = 1.38 + 0.01/\lambda^2$ [λ in µm], obtained for a millimeter-thick PDMS film supported on a Si substrate.

Supporting Information

Supporting Information is available from the Wiley Online Library or from the author.

Acknowledgements

W.J.C. and I.F. contributed equally to this work. S.C. was fully supported by an Alexander von Humboldt postdoc fellowship. The authors thank Anik Kumar Ghosh, Takuya Tsuda, and Dr. Petr Formanek at IPF for assistance with the fabrication and electrical characterization of the mechanical gated logic components. The authors sincerely acknowledge Dr. Quinn A. Besford for valuable scientific discussions. The authors are grateful to Minji Cho for the graphical editing of all figures. A.F. acknowledges support from the German Science Foundation with SPP 2100, project number 404941515. This work was supported in part by German Research Foundation (DFG) Grants MA 5144/9-1, MA 5144/13-1, MA 5144/28-1 and the Helmholtz Association of German Research Centres in the context of the Helmholtz Innovation Lab "FlexiSens" (HIL-A04).

Open access funding enabled and organized by Projekt DEAL.

Conflict of Interest

The authors declare no conflict of interest.

Data Availability Statement

The data that support the findings of this study are available from the corresponding author upon reasonable request.

Keywords

logic gates, strain-gated electric switches, stretchable circuits, thin films, tunneling

Received: June 22, 2021
Revised: July 18, 2021
Published online: September 5, 2021

[1] W. F. Brinkman, D. E. Haggan, W. W. Troutman, *IEEE J. Solid-State Circuits* **1997**, *32*, 1858.
[2] S. H. Byun, J. Y. Sim, Z. Zhou, J. Lee, R. Qazi, M. C. Walicki, K. E. Parker, M. P. Haney, S. H. Choi, A. Shon, G. B. Gereau, J. Bilbily, S. Li, Y. Liu, W. H. Yeo, J. G. McCall, J. Xiao, J. W. Jeong, *Sci. Adv.* **2019**, *5*, eaay0418.
[3] D. H. Kim, R. Ghaffari, N. Lu, J. A. Rogers, *Annu. Rev. Biomed. Eng.* **2012**, *14*, 113.
[4] S. C. B. Mannsfeld, B. C. K. Tee, R. M. Stoltenberg, C. V. H. H. Chen, S. Barman, B. V. O. Muir, A. N. Sokolov, C. Reese, Z. Bao, *Nat. Mater.* **2010**, *9*, 859.
[5] C. Wang, D. Hwang, Z. Yu, K. Takei, J. Park, T. Chen, B. Ma, A. Javey, *Nat. Mater.* **2013**, *12*, 899.
[6] K. K. Kim, S. Hong, H. M. Cho, J. Lee, Y. D. Suh, J. Ham, S. H. Ko, *Nano Lett.* **2015**, *15*, 5240.
[7] T. Q. Trung, N. E. Lee, *Adv. Mater.* **2016**, *28*, 4338.
[8] S. Lee, A. Reuveny, J. Reeder, S. Lee, H. Jin, Q. Liu, T. Yokota, T. Sekitani, T. Isoyama, Y. Abe, Z. Suo, T. Someya, *Nat. Nanotechnol.* **2016**, *11*, 472.
[9] S. I. Rich, R. J. Wood, C. Majidi, *Nat. Electron.* **2018**, *1*, 102.
[10] C. Larson, B. Peele, S. Li, S. Robinson, M. Totaro, L. Beccai, B. Mazzolai, R. Shepherd, *Science* **2016**, *351*, 1071.
[11] C. El Helou, P. R. Buskohl, C. E. Tabor, R. L. Harne, *Nat. Commun.* **2021**, *12*, 1633.
[12] J. Lee, S. Kim, J. Lee, D. Yang, B. C. Park, S. Ryu, I. Park, *Nanoscale* **2014**, *6*, 11932.
[13] H. J. Kim, A. Thukral, C. Yu, *ACS Appl. Mater. Interfaces* **2018**, *10*, 5000.
[14] S. Chen, Y. Wei, X. Yuan, Y. Lin, L. Liu, *J. Mater. Chem. C* **2016**, *4*, 4304.

[15] H. Park, D. S. Kim, S. Y. Hong, C. Kim, J. Y. Yun, S. Y. Oh, S. W. Jin, Y. R. Jeong, G. T. Kim, J. S. Ha, *Nanoscale* **2017**, *9*, 7631.
[16] D. Cho, J. Park, J. Kim, T. Kim, J. Kim, I. Park, S. Jeon, *ACS Appl. Mater. Interfaces* **2017**, *9*, 17369.
[17] G. Cai, J. Wang, K. Qian, J. Chen, S. Li, P. S. Lee, *Adv. Sci.* **2017**, *4*, 1600190.
[18] L. Nela, J. Tang, Q. Cao, G. Tulevski, S. J. Han, *Nano Lett.* **2018**, *18*, 2054.
[19] S. Gong, L. W. Yap, B. Zhu, Q. Zhai, Y. Liu, Q. Lyu, K. Wang, M. Yang, Y. Ling, D. T. H. Lai, F. Marzbanrad, W. Cheng, *Adv. Mater.* **2019**, *31*, 1903789.
[20] Y. Cheng, R. Wang, H. Zhai, J. Sun, *Nanoscale* **2017**, *9*, 3834.
[21] Y. Kim, J. Zhu, B. Yeom, M. Di Prima, X. Su, J. G. Kim, S. J. Yoo, C. Uher, N. A. Kotov, *Nature* **2013**, *500*, 59.
[22] M. Park, J. Im, M. Shin, Y. Min, J. Park, H. Cho, S. Park, M. B. Shim, S. Jeon, D. Y. Chung, J. Bae, J. Park, U. Jeong, K. Kim, *Nat. Nanotechnol.* **2012**, *7*, 803.
[23] N. Matsuhisa, D. Inoue, P. Zalar, H. Jin, Y. Matsuba, A. Itoh, T. Yokota, D. Hashizume, T. Someya, *Nat. Mater.* **2017**, *16*, 834.
[24] N. Matsuhisa, M. Kaltenbrunner, T. Yokota, H. Jinno, K. Kuribara, T. Sekitani, T. Someya, *Nat. Commun.* **2015**, *6*, 7461.
[25] H. Stoyanov, M. Kollosche, S. Risse, R. Waché, G. Kofod, *Adv. Mater.* **2013**, *25*, 578.
[26] T. Sekitani, Y. Noguchi, K. Hata, T. Fukushima, T. Aida, T. Someya, *Science* **2008**, *321*, 1468.
[27] K. Y. Chun, Y. Oh, J. Rho, J. H. Ahn, Y. J. Kim, H. R. Choi, S. Baik, *Nat. Nanotechnol.* **2010**, *5*, 853.
[28] L. Duan, D. R. D'hooge, L. Cardon, *Prog. Mater. Sci.* **2020**, *114*, 100617.
[29] S. Biccai, C. S. Boland, D. P. O'Driscoll, A. Harvey, C. Gabbett, D. R. O'Suilleabhain, A. J. Griffin, Z. Li, R. J. Young, J. N. Coleman, *ACS Nano* **2019**, *13*, 6845.
[30] Z. Yang, Y. Pang, X. L. Han, Y. Yang, Y. Yang, J. Ling, M. Jian, Y. Zhang, T. L. Ren, *ACS Nano* **2018**, *12*, 9134.
[31] K. Zhao, W. Niu, S. Zhang, *J. Mater. Sci.* **2020**, *55*, 2439.
[32] S. Wang, D. D. L. Chung, *J. Mater. Sci.* **2007**, *42*, 4987.
[33] T. Ouchi, R. C. Hayward, *ACS Appl. Mater. Interfaces* **2020**, *12*, 10031.
[34] G. Lee, T. Lee, Y. W. Choi, P. V. Pikhitsa, S. J. Park, S. M. Kim, D. Kang, M. Choi, *J. Mater. Chem. C* **2017**, *5*, 10920.
[35] B. Xu, D. Chen, R. C. Hayward, *Adv. Mater.* **2014**, *26*, 4381.
[36] J. G. Simmons, *J. Appl. Phys.* **1963**, *34*, 1793.
[37] M. Todeschini, A. Bastos da Silva Fanta, F. Jensen, J. B. Wagner, A. Han, *ACS Appl. Mater. Interfaces* **2017**, *9*, 37374.
[38] T. Tsujioka, A. Nishimura, *Appl. Phys. A* **2021**, *127*, 228.
[39] L. Tang, J. Shang, X. Jiang, *Sci. Adv.* **2021**, *7*, eabe3778.
[40] Y. Wang, S. Lee, T. Yokota, H. Wang, Z. Jiang, J. Wang, T. Someya, *Sci. Adv.* **2020**, *6*, eabb7043.